

Main Manuscript for

Model-agnostic network inference enhancement from noisy measurements via curriculum learning

Kai Wu^a, Yuanyuan Li^b, Jing Liu^b

^aSchool of Artificial Intelligence, Xidian University, Xi'an 710071, China; ^bGuangzhou Institute of Technology, Xidian University, Guangzhou 510555, China

*Jing Liu.

Email: neouma@mail.xidian.edu.cn

Author Contributions: K.W., J.L., and Y.L. designed research; Y.L. and K.W. performed research; K.W. and Y.L. analyzed data; and Y.L. and K.W. wrote the paper.

Competing Interest Statement: The authors declare no conflict of interest.

Classification: Physical Sciences, Applied Mathematics

Keywords: network inference, curriculum learning, noise, time series

This PDF file includes:

Main Text
Figures 1 to 4

Abstract

Noise is a pervasive element within real-world measurement data, significantly undermining the performance of network inference models. However, the quest for a comprehensive enhancement framework capable of bolstering noise resistance across a diverse array of network inference models has remained elusive. Here, we present an elegant and efficient framework tailored to amplify the capabilities of network inference models in the presence of noise. Leveraging curriculum learning, we mitigate the deleterious impact of noisy samples on network inference models. Our proposed framework is model-agnostic, seamlessly integrable into a plethora of model-based and model-free network inference methods. Notably, we utilize one model-based and three model-free network inference methods as the foundation. Extensive experimentation across various synthetic and real-world networks, encapsulating diverse nonlinear dynamic processes, showcases substantial performance augmentation under varied noise types, particularly thriving in scenarios enriched with clean samples. This framework's adeptness in fortifying both model-free and model-based network inference methodologies paves the avenue towards a comprehensive and unified enhancement framework, encompassing the entire spectrum of network inference models.

Significance Statement

Inferring networks from observed time series data presents a formidable hurdle across various academic disciplines. Employing network inference techniques offers a clear glimpse into the interconnections among nodes. Nonetheless, these methods have persistently contended with the detrimental effects of noise within time series data, resulting in misguided determinations of link presence. In response, we introduce a model-agnostic enhancement strategy for network inference, with the objective of mitigating noise's impact on these methodologies and realizing substantial performance improvements. Our endeavor represents a crucial advancement in reducing the impact of noise, thereby propelling the quest for precise network inference.

Main Text

Introduction

Complex networks (1), (2) play a pivotal role in comprehending, identifying, and regulating complex systems (3) across diverse domains such as biology (4)-(6), physics (7), and technology (8). In reality, direct access to network structures remains limited, often necessitating inference from measurement data (9). These inference methodologies can be categorized into two primary groups: model-free and model-based. Most model-free techniques establish links between nodes by detecting statistical dependencies within time series data, encompassing correlations, mutual information, Granger causality, transfer entropy, and reservoir computing (10)-(15). However, such approaches might inadvertently uncover indirect interactions among network components, an issue that recent research has sought to address (16). On the other hand, model-based strategies, such as stability selection (17), compressed sensing (7), (18), (19), (20), Bayesian inference (21)-(23), online learning (24), evolutionary computation (25), presuppose a priori knowledge of system behaviors. Yet, the efficacy of existing network inference models experiences significant degradation in the presence of measurement data noise attributed to various uncontrollable factors, such as equipment glitches, sensor inaccuracies, and human-induced perturbations leading to erroneous or absent node information (26) (27). While certain studies have explored the resilience of their network inference methodologies against minor noise levels (7), (18), (19), (28)-(33), they have primarily focused on enhancing individual inference methods, lacking broader applicability to other techniques.

This article presents a model-agnostic framework, named MANIE, designed to enhance network inference across both model-based and model-free paradigms when confronted with noisy measurement data. The presence of noise can divert the optimization process of network inference

models from the optimal trajectory exhibited by clean samples. Our approach aims to address this challenge by attenuating the influence of noisy samples on network inference models. Leveraging curriculum learning techniques (35)-(38), we progressively identify and downweight noisy samples within the network inference process. The simplicity of the MANIE framework lies in its reliance on weighted samples, enabling seamless integration into existing network inference models. Remarkably, MANIE offers broader support for diverse network inference methodologies compared to existing strategies. Notably, its efficiency shines through, yielding significant performance improvements across a spectrum of noisy scenarios.

Results

Overview of the MANIE framework

Given the measurement data Y , the aim of network reconstruction is to accurately recover the network structure A . Figure 1 demonstrate the graphical illustration of MANIE framework. Firstly, we initialize the vector of weights $\mathbf{v}^0 = [v_1, v_2, \dots, v_M]^T \in [0, 1]^M$, and the network structure A^0 , along with the training scheduler λ , where M represents the sample size. The loss function is the sum of contributions from each sample, and \mathbf{v} allows for adjusting the contribution of each sample to the loss function. With Y , \mathbf{v}^t , and A^t given, we can employ existing network reconstruction methods to obtain the network structure A^{t+1} . Subsequently, based on A^{t+1} , \mathbf{v}^t , and λ , we use curriculum learning to update \mathbf{v}^{t+1} , readjusting the contribution of each sample to the loss function. This iterative process continues until convergence (\mathbf{v} hardly changes), yielding the final target network structure A .

To demonstrate the resilience of our methodology in elucidating direct interactions, we applied it to a range of systems manifesting heterogeneous collective dynamics. These encompassed gene regulation and Kuramoto-like oscillators for model-free network inference, alongside evolutionary game (EG) models and epidemic spread within human society for model-based network inference, all conducted within varied noisy settings. We executed reconstruction techniques for each network unit. Within this investigation, we adopted the area under the receiver-operating-characteristic curve (AUC) score as the conventional metric for evaluating inference quality, with a higher AUC score denoting superior inference performance.

Model-free network inference enhancement

We initially consider a paradigmatic model-free network inference approach, ARNI (Algorithm for Revealing Network Interactions) (16), as an illustrative example to showcase the efficacy of the proposed MANIE framework. We undertake systematic reconstructions of the Zachary's karate club (ZK) network (45) and the directed random network based on Kuramoto-like oscillators (46), subject to varying levels of noise. Furthermore, to demonstrate the performance of MANIE in practical scenarios, we employ a blinded, community-wide DREAM4 in silico network inference challenge (5) and the Millar 10 network (47). Specific parameter configurations are elaborated upon in the supplementary materials.

Figure 2 demonstrates the substantial performance advancements achieved by MANIE across all scenarios, with a particularly noteworthy enhancement observed in the Millar10 case. The experimental outcomes obtained from the two Kuramoto-like oscillators reveal the vulnerability of ARNI to noise, leading to noticeable degradation in performance. Additionally, MANIE proves its capacity to augment ARNI's efficacy even under noise-free conditions, although the extent of improvement is relatively less than that in noisy scenarios. Notably, data can be categorized into challenging and facile samples, each exerting varying influences on ARNI's performance. Through judicious weight adjustments, MANIE effectively attenuates the impact of challenging samples on ARNI, consequently elevating its performance. Moreover, our observations reveal that reconstructions tend to be superior in scenarios marked by the presence of clean samples, such as noise_v2 and noise_v3, whereas the absence of clean samples characterizes the noise_v1

scenario. To conclude, MANIE is aptly suited for enhancing the performance of model-free network inference methodologies, resulting in substantial performance enhancements.

Model-based network inference enhancement

We proceed to assess the efficacy of MANIE in the context of model-based network inference methods. To demonstrate its versatility, we apply MANIE to prototypical systems, specifically evolutionary game (EG) models, as well as two epidemic spreading models—namely, the classic susceptible-infected-susceptible (SIS) dynamics (48) and contact processes (CP) (49). It becomes evidently apparent that the performance of model-based methods experiences a notable decline in the presence of noise. To accommodate diverse noise scenarios, we introduce two variations of MANIE: 1) MANIEv1, where each sample's weight v is computed based on its individual loss; 2) MANIEv2, wherein samples at the same time step share the weight, calculated as the average loss value at that moment.

Evolutionary Game model

Complex dynamical systems across biology, social sciences, and economics find representation in EG models (50), (51). Leveraging payoff and strategy data from prisoner's dilemma games, we adopt two prevalent sparse regression methods—namely, LASSO (39) and sequential threshold ridge regression (STRidge) (40)—as baseline techniques to independently identify the neighboring node sets in a straightforward manner. Derived from established research (39), (40), these two strategies, LASSO and STRidge, are separately incorporated into MANIE. In the context of the EG model, we introduce random noise to clean data, albeit with slight yet meaningful variations: (i) noise_free: time series devoid of noise; (ii) noise_v1: random noise with an amplitude of 10 added to each time step's recordings, with a probability of 0.5; (iii) noise_v2: random noise with amplitudes less than 10, added to each time step's recordings with a probability of 0.5; (iv) noise_v3: random noise added to the global data, magnitudes set at 1, 5, and 10 respectively, with the final outcomes averaged. The experimental findings are presented in Figure 2(b)(c).

In noise-free scenarios, MANIE is at least as capable as STRidge and LASSO, and in some cases, even exhibits a slight advantage over them. When noise is present, MANIE consistently achieves greater performance improvement compared to LASSO and STRidge. In noise_v1 and noise_v2 scenarios, MANIEv2 significantly outperforms MANIEv1. In the case of noise_v3, MANIEv2 maintains a slight performance advantage over MANIEv1. Consequently, MANIEv2 demonstrates broader applicability than MANIEv1. For situations involving unknown noise conditions, we recommend the preference for MANIEv2.

Epidemic spreading in the human society

The identification, prediction, and control of epidemic spreading in human society or information diffusion on computer networks are complex interdisciplinary challenges. Here, the network inference method (referred to as CS) and the examples draw from established research (19). We then integrate CS into the MANIE framework. For the case of epidemic spreading in human society, we consider binary time series reversal as well as the presence of hidden units mediating indirect interactions. We introduce two common types of noise: (i) noise_free, which represents binary time series without noise; (ii) noise_v1, where 10% of nodes in the binary time series are missing; (iii) noise_v2, wherein each record is misremembered with a probability of 0.1, causing a reversal between 0 and 1. The experimental outcomes are depicted in Figure 2(d)(e). In both SIS and CP scenarios, MANIE notably improves the performance of CS. Remarkably, it achieves equivalent enhancement even under noise-free conditions. The hierarchy of noise impact on MANIE, based on strength, is as follows: noise_v1 < noise_v2.

Impact of noise level on MANIE

In Figure 3(a)(c), as noise intensity escalates, the performance of both MANIE and the embedded network inference methods experiences a gradual decline, accentuating the growing effectiveness of MANIE. As illustrated in Figure 3(b)(d), as the proportion of noisy data increases, the

performance of both MANIE and the embedded network inference methods witnesses a diminishing pattern. What remains clear is that, irrespective of fluctuating noise intensities and proportions of noisy data, MANIE consistently demonstrates enhanced noise resistance. Moreover, this valuable attribute persists in both model-free and model-based contexts.

Visualization of learned ν

We visualize the learned ν values, observing that during the optimization process, the ν values linked to noisy samples tend to decrease. This signifies that MANIE adeptly alleviates the influence of noisy samples on network reconstruction. Concurrently, the ν values connected to the majority of clean samples tend to increase, showcasing MANIE's proficiency in safeguarding the contribution of clean samples to the loss function.

Discussion

Noise of varying magnitudes can emerge within the sampled measurement data, and our method demonstrates resilience in such scenarios. With increasing time series length and the incorporation of diverse short series compositions in non-periodic dynamics, enhanced reconstruction quality is observed. In contrast to exhaustive state space sampling, our approach effectively mitigates noise's impact, enhancing performance while maintaining sampling and storage efficiency, especially when recording availability is limited. The inference of directed links among all units yields the network's intrinsic topology, enabling parallel computation in real-world networks. Notably, our approach remains practically viable even when only a portion of the network is captured.

MANIE consistently matches or surpasses the embedded network inference methods, a conclusion demonstrated across multiple cases. It is notably effective in scenarios featuring clean data samples. Crucially, MANIE exhibits significant performance improvement even under noise-free and global noise conditions. Our framework's versatility encompasses a wide array of network reconstruction contexts, encompassing model-free and model-based models. It remains straightforward and adaptable, making integration into existing network reconstruction methods seamless.

However, MANIE's enhancement capacity is confined to certain network inference method types. A prerequisite for our method's implementation is the availability of sample contributions to the loss function, a condition incompatible with measures such as mutual information, Granger causality, and transfer entropy. This presents an avenue for future refinement.

In summary, our framework systematically bolsters the noise resistance of model-based and model-free network inference methods, rectifying an overlooked facet. Thanks to its simplicity, adaptability, and efficiency, this proposed framework holds potential for expansive applications.

Methods

Problem formulation

A time series dataset comprises a sequence of random variables indexed over time, encapsulating intricate insights into direct interactions within networks. To comprehend the mapping of unit dynamics onto direct interactions, consider a system governed by the differential equation:

$$\dot{x} = \mathbf{F}(\mathbf{A}, \mathbf{x}(t)) + \xi(t)$$

where $\mathbf{x}(t) = [x_1(t), \dots, x_N(t)] \in \mathbb{R}^N$ is the state of units, $\dot{x} = dx(t)/dt$ denotes its temporal derivative, \mathbf{A} denotes the network structure among units, $\mathbf{F}: \mathbb{R}^N \rightarrow \mathbb{R}^N$ stands for an unknown nonlinear function that indicates direct interactions among those units, and $\xi(t) = [\xi_1(t), \dots, \xi_N(t)] \in \mathbb{R}^N$ defines the external noise. Network inference aims to deduce \mathbf{A} from periodic or non-periodic dynamics based on the aforementioned equation.

Model-free network inference enhancement for ARNI

This section outlines the integration of the model-free network inference method ARNI into the MANIE framework. ARNI is a computationally efficient and robust technique built upon the Block

Orthogonal Least Squares (BOLS) algorithm (42). Unlike methods requiring a sparse representation of dynamics or strict statistical dependencies, ARNI offers parallelizability and reliability.

To systematically dissect the dynamics into direct network interactions, we introduce the notions of an explicit dependency matrix and basis function. This approach yields a universal representation for dynamical systems, characterized as follows:

$$\begin{aligned} \dot{x}_i = & \sum_{j=1}^N \Lambda_{jj}^i \sum_{p=1}^{P_1} c_{j,p}^i h_{j,p}(x_j) + \sum_{j=1}^N \sum_{s=1}^N \Lambda_{jj}^i \Lambda_{ss}^i \sum_{p=1}^{P_2} c_{js,p}^i h_{js,p}(x_j, x_s) \\ & + \sum_{j=1}^N \sum_{s=1}^N \sum_{w=1}^N \Lambda_{jj}^i \Lambda_{ss}^i \Lambda_{ww}^i \sum_{p=1}^{P_3} c_{jsw,p}^i h_{jsw,p}(x_j, x_s, x_w) + \dots + \xi_i \end{aligned}$$

where \dot{x}_i denotes the temporal derivative of the state of an arbitrary unit i , N is the number of units

in the system, diagonal matrices $\Lambda_{jj}^i = \begin{cases} 0 & \text{if } \frac{\partial F_i}{\partial x_j} \equiv 0 \\ 1 & \text{if } \frac{\partial F_i}{\partial x_j} \neq 0 \end{cases}$ indicates whether a unit j directly acts on unit

i or not, h stands for basis functions, P indicates the number of basis functions employed in the expansion, c stands for the unknown coefficient, and ξ_i represents external noise acting on unit i . ARNI returns a ranked list of interactions for units indicating the order of neighbors identified by iteratively minimizing orthogonal projections on composite function spaces. While finding the sequentially-enlarged function space, the criterion is defined as the standard deviation of the projection-error vector computed by the given unit's whole time series dataset. Fundamentally, noise complicates the inference process owing to its abnormal projection-error. We adjust the weight of each projection-error in the calculation of criteria, so as to weaken the negative influence of noise. As the optimization, an increasing number of time series is incorporated into the learning process and the weight of noise is much smaller than that of clean data. This strategy can effectively deal with the random occurrence of noise over time.

The detailed algorithmic process is shown below. The **bold** sections represent the parts where our approach differs from ARNI, demonstrating how the MANIE framework can be seamlessly integrated into ARNI.

1. Choose orders K and select models for basis functions $h_{j,p}(x_j)$, $h_{js,p}(x_j, x_s)$, $h_{jsw,p}(x_j, x_s, x_w)$, and so on.
2. Compute vectors $\dot{x}_i = [\dot{x}_{i,1}, \dot{x}_{i,2}, \dots, \dot{x}_{i,M}] \in \mathbb{R}^M$ for all i and construct the set of matrices \mathcal{H} up to chosen K , where \mathcal{H} is defined as $\mathcal{H} := \{H_q | q = 1, 2, \dots, Q\}$, where $H_{N+j} := H_{jj}$, $H_{N+N^2+j} := H_{jjj}$, and so on, and $Q = \sum_{k=1}^K N^k$.
3. Define the set $\mathcal{N} := \{1, 2, \dots, S\}$ that contains all s indices of \mathcal{H} .
4. **Initialize the vector of weights** $\mathbf{v} = [v_1, v_2, \dots, v_M]^T \in [0, 1]^M$ **and the training scheduler** $\lambda = \lambda_0$.
5. Define the set of incoming interactions of unit i at the l -th iteration as $\hat{\mathcal{L}}_{i,l}$, and initialize $\hat{\mathcal{L}}_{i,0} = \emptyset$.
6. Compute $\forall n \in \mathcal{N} \setminus \hat{\mathcal{L}}_{i,(l-1)}$ and the projection-error function $\epsilon(\hat{\mathcal{L}}_{i,l}^n) := \sigma((\dot{x}_i - H_{\hat{\mathcal{L}}_{i,l}^n}^\dagger H_{\hat{\mathcal{L}}_{i,l}^n} \dot{x}_i) \cdot \mathbf{v}^T)$, where $\sigma(\mathbf{y})$ stands for the standard deviation of entries of \mathbf{y} , \dagger indicates the Moore-Penrose pseudo-inverse, $\hat{\mathcal{L}}_{i,l}^n = \hat{\mathcal{L}}_{i,(l-1)} \cup \{n\}$ and $H_{\hat{\mathcal{L}}_{i,l}^n} := [H_{j_1}, H_{j_2}, \dots, H_{j_{l-1}}, H_n]^T \in \mathbb{R}^{lP \times M}$, where $j_p \in \hat{\mathcal{L}}_{i,(l-1)}$ and $p = \{1, 2, \dots, l-1\}$.
7. Store results in $\epsilon_i(l) \in \mathbb{R}^L$ where $[\epsilon_i(l)]_r = \epsilon(\hat{\mathcal{L}}_{i,l}^{n_r})$, $n_r \in \mathcal{N} \setminus \hat{\mathcal{L}}_{i,(l-1)}$, $r \in \{1, 2, \dots, L\}$ and $L = |\mathcal{N} \setminus \hat{\mathcal{L}}_{i,(l-1)}|$.

8. If the standard deviation $\sigma_i := \sigma(\epsilon_i(l)) \leq \theta$, **compute the difficulty measurer** $loss = \text{abs}(\hat{\mathbf{x}}_i - H_{\hat{\mathcal{L}}_{i,(l-1)}}^\dagger H_{\hat{\mathcal{L}}_{i,(l-1)}} \hat{\mathbf{x}}_i)^T$. Else, **UPDATE** $\hat{\mathcal{L}}_{i,l} = \hat{\mathcal{L}}_{i,(l-1)} \cup \{n^*\}$ where $n^* = \text{arg} \min_{n \in \mathcal{N} \setminus \hat{\mathcal{L}}_{i,(l-1)}} (\epsilon(\hat{\mathcal{L}}_{i,l}^n))$ and **REPEAT** from steps 6 and 7 until the condition in step 8 is satisfied or $\mathcal{N} \setminus \hat{\mathcal{L}}_{i,(l-1)} = \emptyset$.
9. **Compute** $\mathbf{v} = \mathbf{v}^*(loss, \lambda)$ **and their closed-form solutions can be seen in Eq. 2**. If the vector \mathbf{v} remains constant, **STOP** algorithm and **RETURN** $\hat{\mathcal{L}}_{i,(l-1)}$ as set of incoming interactions. **Else, UPDATE** λ **to a larger value to include harder data and REPEAT** from steps 5, 6, 7 and 8 until the condition in step 9 is satisfied.

Model-based network inference enhancement

Through data processing, the general model-based network inference model is given by the following equation

$$\mathbf{Y}_i = \mathbf{F}(\mathbf{X}_i \cdot \mathbf{A}_i), i = 1, 2, \dots, N$$

where $\mathbf{A}_i \in \mathbb{R}^{N \times 1}$ is an adjacency vector that indicates the direct interactions among unit i and other units in the network, $\mathbf{Y}_i \in \mathbb{R}^{M \times 1}$ and $\mathbf{X}_i \in \mathbb{R}^{M \times N}$ are both extracted from time series data. The objective often centers on reconstructing \mathbf{A}_i from \mathbf{Y}_i and \mathbf{X}_i to reveal the neighbors of unit i . Various algorithms developed over the past decades effectively address this challenge, including sparse regression (39) and compressed sensing (59), (60). They commonly serve the capacity of leading to approach the optimal solution by searching from the current solution. Obviously, noise inevitably poses a challenge to update the gradient during the iterations, thereby masking the true network interactions. Moreover, the measurement of all units in a network is not always completely accessible, and thus the recovery of indirect interactions may be promoted by the correlating or decorrelating effects. The goal-orientation of MANIE is to correct for deviated gradient directions by scaling the contribution of each data in loss functions. To be concrete, casting the problem of reconstructing networks into the following form leveraged by sparse regression

$$\min \sum_{i=1}^M v_i loss_i + g(\mathbf{v}; \lambda) = \sum_{i=1}^M \frac{1}{2} v_i (\mathbf{F}(\mathbf{X}_i \mathbf{A}_i) - \mathbf{Y}_i)^2 + \alpha \|\mathbf{A}\|_p + g(\mathbf{v}; \lambda)$$

where $loss_i, i = 1, 2, \dots, M$ stands for associated loss of each instance, $\|\mathbf{A}\|_p$ is the L_p norm of \mathbf{A} , $\alpha > 0$ is the regularization parameter, and $g(\mathbf{v}; \lambda)$ is defined as the self-paced regularizer (43) (44) pertaining to curriculum learning. This problem is solved by adopting an alternative optimization strategy (AOS), which is convergent (44). By jointly learning the network structure \mathbf{A} and the latent weight \mathbf{v} by AOS with gradually increasing age parameter, more samples can be automatically included in the training from noisy to clean in a purely self-paced way.

If we denote \mathbf{A}^k as the k th iteration of the AOS implementation on solving the above problem, and then its two alternative search steps in the next iteration can be described as follows:

1. Calculate \mathbf{v} by solving the following problem under fixed \mathbf{A}^k with the corresponding $g(v_i; \lambda)$:
$$v_i^* = \text{arg} \min_{v_i \in [0,1]} v_i loss_i + g(v_i; \lambda), i = 1, 2, \dots, M \quad (1)$$

The closed-form solutions of Eq.1 can be seen in Eq.2.

2. Update \mathbf{A}^k under fixed \mathbf{v} by optimizing the following

$$\text{arg} \min \sum_{i=1}^M \frac{1}{2} v_i (\mathbf{F}(\mathbf{X}_i \mathbf{A}_i) - \mathbf{Y}_i)^2 + \alpha \|\mathbf{A}\|_p$$

In close analogy to the L_2 norm used in STRidge (40), the substituted L_1 norm in LASSO (39) is also feasible. An alternative is the primal-dual interior point method (41), where it is not necessarily advantageous to have more training data.

Closed-form solutions of \mathbf{v}^* and \mathbf{A}^*

Here, $g(\mathbf{v}; \lambda) = \frac{1}{2} \lambda \sum_{i=1}^M (v_i^2 - 2v_i)$ (52), then the corresponding close-formed solution is

$$v_i^* = \begin{cases} 1 - loss_i/\lambda, & \text{if } loss_i < \lambda \\ 0, & \text{otherwise} \end{cases} \quad (2)$$

If the optimizer is STRidge, the corresponding close-formed solution is:

$$\begin{aligned}
\mathbf{A}^* &= \arg \min_{\mathbf{A}} \frac{1}{M} \sum_{i=1}^M v_i (\mathbf{A}_i \mathbf{X}_i - \mathbf{Y}_i)^2 + \alpha \|\mathbf{A}\|_2^2 \\
&= \arg \min_{\mathbf{A}} \frac{1}{M} \text{tr} \left\{ [(\mathbf{A}\mathbf{X} - \mathbf{Y})^T (\mathbf{A}\mathbf{X} - \mathbf{Y})]_* \begin{bmatrix} v_1 & 0 & 0 \\ 0 & \ddots & 0 \\ 0 & 0 & v_M \end{bmatrix} \right\} + \alpha \|\mathbf{A}\|_2^2 \\
&= [\mathbf{A}^T (\mathbf{A}_* \mathbf{v}) + M\alpha \mathbf{I}]^{-1} [\mathbf{A}^T (\mathbf{Y}_* \mathbf{v})]
\end{aligned}$$

Acknowledgments

This work was supported in part by the National Natural Science Foundation of China under Grant 62206205, in part by the Guangdong High-level Innovation Research Institution Project under Grant 2021B0909050008, and in part by the Guangzhou Key Research and Development Program under Grant 202206030003.

References

1. Newman, M. E. J. The structure and function of complex networks. *SIAM Rev.* 45, 167–256 (2003).
2. Boccaletti, S., Latora, V., Moreno, Y., Chavez, M. & Hwang, D. U. Complex networks: Structure and dynamics. *Phys. Rep.* 424, 175–308 (2006).
3. Fan, C., Zeng, L., Sun, Y. et al. Finding key players in complex networks through deep reinforcement learning. *Nat. Mach. Intell.* 2, 317–324 (2020).
4. Gardner, T. S., di Bernardo, D., Lorenz, D. & Collins, J. J. Inferring genetic networks and identifying compound mode of action via expression profiling. *Science* 301, 102–105 (2003).
5. Marbach, D. et al. Revealing strengths and weaknesses of methods for gene network inference. *Proc. Natl. Acad. Sci. USA* 107, 6286–6291 (2010).
6. Marbach, D. et al. Wisdom of crowds for robust gene network inference. *Nat. Methods* 9, 796–804 (2012).
7. Nitzan, M., Casadiego, J., & Timme, M. Revealing physical interaction networks from statistics of collective dynamics. *Sci. Adv.* 3, e1600396 (2017).
8. Menck, P. J., Heitzig, J., Kurths, J. & Schellnhuber H. J. How dead ends undermine power grid stability. *Nat. Commun.* 5, 3969 (2014).
9. Wang, W. X., Lai, Y. C., & Grebogi, C. Data based identification and prediction of nonlinear and complex dynamical systems. *Phys. Rep.*, 644, 1–76 (2016).
10. Butte, A.J. & Kohane, I.S. Mutual information relevance networks: functional genomic clustering using pairwise entropy measurements. *Pac. Symp. Biocomput.* 2000, 418–429 (2000).
11. Margolin, A.A. et al. ARACNE: an algorithm for the reconstruction of gene regulatory networks in a mammalian cellular context. *BMC Bioinformatics* 7 (suppl. 1), S7 (2006).
12. Granger, C. W. J. Investigating causal relations by econometric models and cross-spectral methods. *Econometrica* 37, 424–438 (1969).
13. J. Runge, J. Heitzig, V. Petoukhov, and J. Kurths, Escaping the curse of dimensionality in estimating multivariate transfer entropy, *Phys. Rev. Lett.* 108, 258701 (2012).
14. Banerjee, A., Hart, J. D., Roy, R., & Ott, E. Machine learning link inference of noisy delay-coupled networks with optoelectronic experimental tests. *Phys. Rev. X* 11(3), 031014 (2021).
15. J. Sun, D. Taylor, and E. M. Bollt, Causal network inference by optimal causation entropy, *SIAM J. Appl. Dyn. Syst.* 14, 73 (2015).
16. Casadiego, J., Nitzan, M., Hallerberg, S. et al. Model-free inference of direct network interactions from nonlinear collective dynamics. *Nat. Commun.* 8, 2192 (2017).
17. Haury, A. C., Mordelet, F., Vera-Licona, P., & Vert, J. P. TIGRESS: trustful inference of gene regulation using stability selection. *BMC Syst. Biol.* 6(1), 1–17 (2012).

18. X. Han, Z. Shen, W.-X. Wang, and Z. Di, Robust Reconstruction of Complex Networks from Sparse Data, *Phys. Rev. Lett.* 114, 028701 (2015).
19. Z. Shen, W.-X. Wang, Y. Fan, Z. Di, and Y.-C. Lai, Reconstructing propagation networks with natural diversity and identifying hidden sources, *Nat. Commun.* 5, 4323 (2014).
20. Wang, W. -X., Lai, Y. -C., Grebogi, C. & Ye, J. Network reconstruction based on evolutionary-game data via compressive sensing. *Phys. Rev. X* 1, 021021 (2011).
21. Peixoto, T. P. Network reconstruction and community detection from dynamics. *Phys. Rev. Lett.* 123(12), 128301 (2019).
22. M. E. J. Newman, Network structure from rich but noisy data, *Nat. Phys.* 14, 542 (2018).
23. Wang, H., Ma, C., Chen, H.S. et al. Full reconstruction of simplicial complexes from binary contagion and Ising data. *Nat. Commun.* 13, 3043 (2022).
24. Wu, K., Hao, X., Liu, J., Liu, P., & Shen, F. Online reconstruction of complex networks from streaming data. *IEEE T. Cybernetics*, 52(6), 5136–5147, (2022).
25. Wu, K., Liu, J., Hao, X., Liu, P., & Shen, F. An evolutionary multiobjective framework for complex network reconstruction using community structure. *IEEE T. Evolut. Comput.*, 25(2), 247–261 (2021).
26. Peel, L., Peixoto, T. P., & De Domenico, M. Statistical inference links data and theory in network science. *Nat. Commun.* 13, 6794 (2022).
27. Banerjee, A., Chandra, S., & Ott, E. Network inference from short, noisy, low time-resolution, partial measurements: Application to *C. elegans* neuronal calcium dynamics. *Proc. Natl. Acad. Sci. USA* 120(12), e2216030120 (2023).
28. Gao, TT., Yan, G. Autonomous inference of complex network dynamics from incomplete and noisy data. *Nat. Comput. Sci.* 2, 160–168 (2022).
29. Aalto, A., Viitasaari, L., Ilmonen, P. et al. Gene regulatory network inference from sparsely sampled noisy data. *Nat. Commun.* 11, 3493 (2020).
30. T. P. Peixoto, Reconstructing networks with unknown and heterogeneous errors, *Phys. Rev. X* 8, 041011 (2018).
31. Young, J. G., Cantwell, G. T., & Newman, M. E. J. Bayesian inference of network structure from unreliable data. *J. Complex Netw.*, 8(6), cnaa046 (2020).
32. Newman, M. E. J. Estimating network structure from unreliable measurements. *Phys. Rev. E* 98, 062321 (2018).
33. Young, J.-G., Valdovinos, F. S. & Newman, M. E. J. Reconstruction of plant-pollinator networks from observational data. *Nat. Commun.* 12, 3911 (2021).
34. Bengio, Y., Louradour, J., Collobert, R., & Weston, J. (2009, June). Curriculum learning. In *Proceedings of the 26th annual international conference on machine learning* (pp. 41-48).
35. Wang, X., Chen, Y., & Zhu, W. A survey on curriculum learning. *IEEE T. Pattern. Anal.*, 44(9), 4555–4576 (2022).
36. Soviany, P., Ionescu, R. T., Rota, P., & Sebe, N. Curriculum learning: A survey. *Int. J. Comput. Vision*, 130(6), 1526–1565 (2022).
37. Guo, J., Fialková, V., Arango, J.D. et al. Improving de novo molecular design with curriculum learning. *Nat. Mach. Intell.* 4, 555–563 (2022).
38. Mokaya, M., Imrie, F., van Hoorn, W.P. et al. Testing the limits of SMILES-based de novo molecular generation with curriculum and deep reinforcement learning. *Nat. Mach. Intell.* 5, 386–394 (2023).
39. Tibshirani, R. Regression shrinkage and selection via the lasso. *J. Roy. Stat. Soc. B Methodol.* 58, 267–288 (1996).
40. Rudy, S. H., Brunton S L, Proctor J L, et al. Data-driven discovery of partial differential equations. *Sci. Adv.* 2017, 3(4): e1602614.
41. Mehrotra, S. On the implementation of a primal-dual interior point method. *SIAM J. Optimiz.*, 1992, 2(4): 575-601.
42. Majumdar, A. & Ward, R. K. Fast group sparse classification. *Can. J. Electr. Comput. Eng.* 34, 136–144 (2009).

43. Kumar, M., Packer, B., & Koller, D. (2010). Self-paced learning for latent variable models. *Advances in neural information processing systems*, 23.
44. Meng, D., Zhao, Q., & Jiang, L. A theoretical understanding of self-paced learning. *Inform. Sciences*, 414, 319–328 (2017).
45. Zachary, W. W. An Information Flow Model for Conflict and Fission in Small Groups. *J. Anthropological Res.* 33, 452–473 (1977).
46. Hansel, D., Mato, G., & Meunier, C. Clustering and slow switching in globally coupled phase oscillators. *Phys. Rev. E*, 48, 3470 (1993).
47. Pokhilko, A., Hodge, S. K., Stratford, K., Knox, K., Edwards, K. D., Thomson, A. W., ... & Millar, A. J. Data assimilation constrains new connections and components in a complex, eukaryotic circadian clock model. *BMC Syst. Biol.*, 6(1), 416 (2010).
48. Pastor-Satorras, R. & Vespignani, A. Epidemic spreading in scale-free networks. *Phys. Rev. Lett.* 86, 3200–3203 (2001).
49. Castellano, C. & Pastor-Satorras, R. Non-mean-field behavior of the contact process on scale-free networks. *Phys. Rev. Lett.* 96, 038701 (2006).
50. Nowak, M. A. and May, R. M. Evolutionary games and spatial chaos," *Nature*, 359, 826–829 (1992).
51. G. Szabó and G. Fath, Evolutionary games on graphs. *Phys. Rep.*, 46, 97–216 (2007).
52. Jiang, L., Meng, D., Mitamura, T., & Hauptmann, A. G. (2014, November). Easy samples first: Self-paced reranking for zero-example multimedia search. In *Proceedings of the 22nd ACM international conference on Multimedia* (pp. 547-556).
53. Erdős P., Rényi A. On random graphs. *Publ. Math. Debrecen*, 6, 290–297 (1959).
54. Barabási A.L., Albert R. Emergence of scaling in random networks *Science*, 286, 509–512 (1999).
55. Newman M.E., Watts D.J. Renormalization group analysis of the small-world network model *Phys. Lett. A*, 263(4), 341–346 (1999).
56. Davis G., Mallat S., Avellaneda M. Adaptive greedy approximations. *Constr. Approx.* 13(1), 57–98 (1997).
57. Girvan, M. & Newman, M. E. Community structure in social and biological networks. *Proc. Natl. Acad. Sci.* 99, 7821–7826 (2002).
58. Lusseau, D. et al. The bottlenose dolphin community of doubtful sound features a large proportion of long-lasting associations. *Behav. Ecol. Sociobiol.* 54, 396–405 (2003).
59. Candès, E. J., Romberg, J. & Tao, T. Robust uncertainty principles: Exact signal reconstruction from highly incomplete frequency information. *IEEE Trans. Inf. Theo.* 52, 489–509 (2006).
60. Candès, E. J. & Wakin, M. B. An introduction to compressive sampling. *Sig. Proc. Mag. IEEE* 25, 21–30 (2008).

Figures and Tables

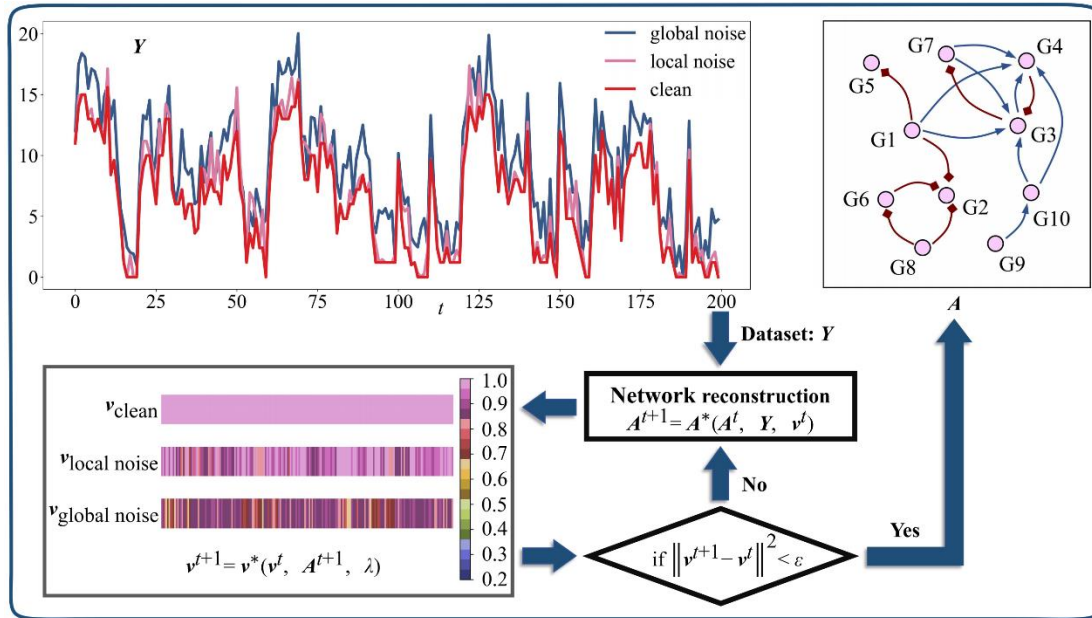


Figure 1. Graphical illustration of MANIE framework based on noisy time series. A^* represents the value of A when the loss function takes its minimum, and similarly, v^* represents the value of v when the loss function takes its minimum. “global noise” refers to all samples being contaminated by noise, while “local noise” indicates that only a portion of the samples is contaminated. “clean” refers to untainted sample data.

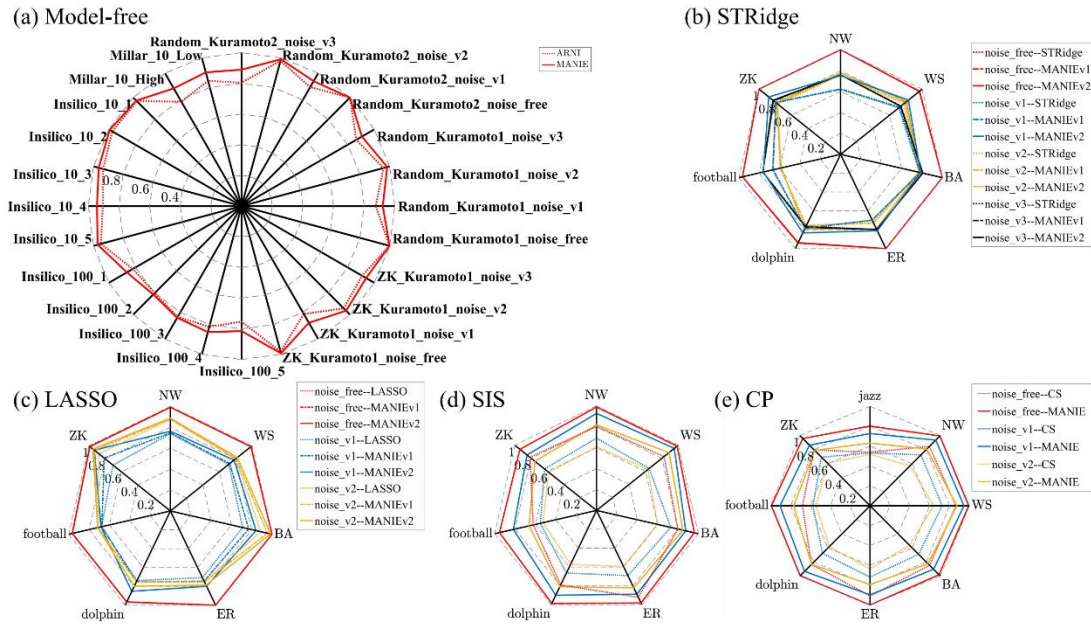


Figure 2. displays the results for various scenarios: (a) AUC scores for model-free network inference from noisy data. Different datasets are utilized, such as Millar_10_Low and Millar_10_High representing stochastic simulations of the Arabidopsis thaliana circadian clock model. Insilico_10 and Insilico_100 pertain to networks of sizes 10 and 100 in the DREAM4 in silico network inference challenge. Similarly, Random_Kuramoto1 and Random_Kuramoto2 depict the dynamics of directed random networks under Kuramoto-1 and Kuramoto-2 oscillators, respectively. ZK_Kuramoto1 illustrates the dynamics of Zachary’s karate club network (ZK) under a Kuramoto-1 oscillator. noise_free signifies time series without noise, while noise_v1, noise_v2, and noise_v3 represent different levels of noise addition. The suffix of noise_v1 represents that white Gaussian noise is added to the global time series with a SNR of 10. The suffix of noise_v2 represents that each timestep the data is recorded, there is white Gaussian noise in terms of the probability 0.5, and the SNR is 10dB. The suffix of noise_v3 represents that each timestep the data is recorded, there is white Gaussian noise in terms of the probability 0.5, and the SNR is 10 dB times a random decimal number from 0 to 1. (b) AUC scores for model-based inference from EG data using the MANIE framework with embedded STRidge. Here, we employ three real-world networks: ZK, football (57), and dolphin (58). Additionally, we utilize four synthetic networks with 40 nodes each: Erdős-Rényi random network (ER) (53), Barabási-Albert scale-free network (BA) (54), Newman-Watts small-world network (NW) (55), and Watts-Strogatz small-world network (WS) (56). Detailed information regarding these networks can be found in the supplementary materials. (c) AUC scores for model-based inference from EG data using the MANIE framework with embedded LASSO. (d) AUC scores for model-based inference of propagation networks for SIS dynamics using the MANIE framework with embedded primal-dual interior point method. CS represents reconstruction with the primal-dual interior point method. (e) AUC scores for model-based inference of propagation networks for CP dynamics using the MANIE framework. The symbolism aligns with scenario (d). These results offer insights into the performance of different methods under diverse conditions. Statistical significance is obtained through multiple Mann–Whitney tests. If a p value of $<10^{-3}$, it means not significant.

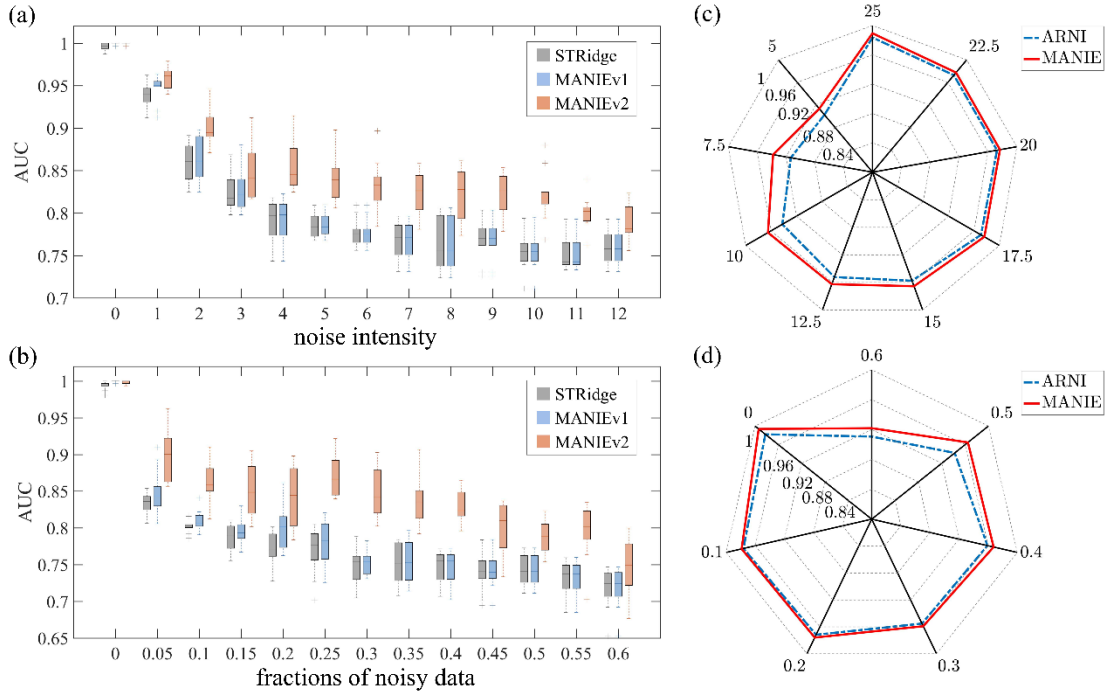


Figure 3. demonstrates the influence of noise levels on MANIE in the context of ZK network reconstruction. (a) AUC scores for model-based inference from EG data using the MANIE framework with embedded STRidge, varying by noise intensity while maintaining a 0.5 fraction of noisy data. (b) AUC scores for model-based inference from EG data using the MANIE framework with embedded STRidge, varying by the fraction of noisy data while keeping the noise intensity at 10. (c) AUC scores for model-free network inference, dependent on the signal-to-noise ratio (SNR)/dB. (d) AUC scores for model-free network inference, influenced by the fraction of noisy data. The EG process underwent 6 repetitions, each encompassing 10 rounds. Model-free data were aggregated through brief transient time series spanning 5 time steps, originating from 50 distinct initial conditions using a Kuramoto-1 oscillator. The "distributed sampling" initial conditions were randomly selected from uniform distributions within interval $[-\pi \ \pi]$.

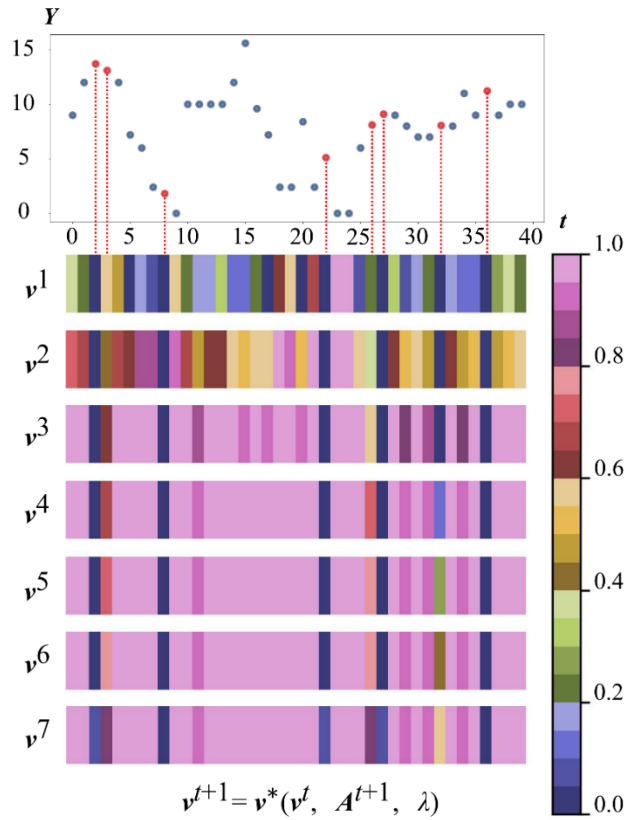


Figure 4. illustrates the weight vector v optimization. Y corresponds to the initial agent's payoff within the ZK network. The EG process was iterated 8 times, with each iteration comprising 5 rounds. Noise was introduced at a fraction of 0.2, with a noise intensity of 5. Clean data is denoted by blue marks, while red marks indicate data affected by noise.

Supporting Information for

Model-agnostic network inference enhancement from noisy measurements via curriculum learning

This PDF file includes:

Supporting text
Figures S1 to S5
SI References

Nonlinear Dynamics

Kuramoto-like oscillators. Kuramoto-like oscillators show the complexity of coupled nonlinear dynamics. The corresponding expression has two Fourier modes

$$\dot{x}_i = w_i + \frac{1}{n_i} \sum_{j=1}^N J_{ij} [\sin(x_j - x_i - 1.05) + 0.33 \sin(2(x_j - x_i))] + \xi_i,$$

where n_i is the incoming connections of node i , N is the number of nodes, and J_{ij} is given by the entry of $J = R \odot A$, where \odot stands for the Hadamard product. Each entry of $R \in \mathbb{R}^{N \times N}$, $R_{ij} \in [0.5, 1]$ is randomly drawn from a uniform distribution. $A \in \{0, 1\}^{N \times N}$ is a randomly generated adjacency matrix with n_i non-zero entries per row. The natural frequency $w_i \in [-2, 2]$ is also randomly drawn from a uniform distribution. ξ_i stands for the white noise imposed on the dynamics of node i . Here, we simulate above nonlinear dynamics as Kuramoto-2 oscillator. A simplified form is defined to be Kuramoto-1 oscillator:

$$\dot{x}_i = w_i + \frac{1}{n_i} \sum_{j=1}^N J_{ij} [\sin(x_j - x_i)] + \xi_i.$$

SIS and CP models. Assuming that the epidemic starts to propagate from several infected nodes. SIS dynamics and CP are separately analyzed owing to their different characteristic. The state of an arbitrary node i is denoted as:

$$S_i = \begin{cases} 0, & \text{susceptible;} \\ 1, & \text{infected.} \end{cases}$$

For SIS dynamics, the probability of node i being infected by its neighbors at time t is given by

$$P_i^{01}(t) = 1 - (1 - \lambda_i)^{\sum_{j=1, j \neq i}^N a_{ij} S_j(t)},$$

where λ_i is the infection rate of node i , a_{ij} is equivalent to 1 if node i connects to j and 0 otherwise, $S_j(t)$ denotes the state of node j at time t , and the superscript 01 stands for the change from susceptible state (0) to infected state (1). The relation of infection probability can be rewritten as

$$\ln[1 - P_i^{01}(t)] = \ln(1 - \lambda_i) \cdot \sum_{j=1, j \neq i}^N a_{ij} S_j(t).$$

For CP dynamics, the infection probability of node i is

$$P_i^{01}(t) = \lambda_i \sum_{j=1, j \neq i}^N a_{ij} S_j(t) / k_i,$$

where k_i is the degree of node i .

Starting with a fraction of infected nodes, we simulated the binary time series according to propagation dynamics. A challenge is that the infection probability at time t cannot be given directly. To construct reconstruction conditions, we estimated $P_i^{01}(t)$ from the node states. For the specific method, refer to reference (1).

EG models. In an EG, at any given round, one agent must select one strategy: defection or cooperation. Taking the Prisoner's Dilemma Game (PDG) as an example, a 2x2 payoff matrix is defined. If both agents choose cooperation/defection, they receive a respective reward Re/Pu . If they choose different strategies, then the defector gets the payoff Te and the collaborator gets the payoff Se . In this article, we define $Re = 1$, $Pu = Se = 0$, $Te = 1.2$, and the normal form for matrix is:

$$P_{PDG} = \begin{pmatrix} Re & Se \\ Te & Pu \end{pmatrix}.$$

The network structure between agents can be defined as an $N \times N$ weighted matrix X :

$$X = \begin{bmatrix} 0 & \cdots & x_{1N} \\ \vdots & \ddots & \vdots \\ x_{N1} & \cdots & 0 \end{bmatrix},$$

where $x_{ij} \in \{0, 1\}$ ($i, j = 1, 2, 3, \dots, N$) represents the connection of node i and j . $x_{ij} = 1$ if node i connects to j , and $x_{ij} = 0$ otherwise. The payoff for each agent i at round t is defined as:

$$Y_i(t) = \sum_{j=1}^N x_{ij} S_j^T(t) P S_j(t),$$

where $S_i^T(t)$ is the strategy of agent i at round t and T stands for "transpose". To maximize the payoff of agent i in the next round, the Fermi rule is adopted to update its strategy:

$$P(S_i \leftarrow S_j) = \frac{1}{1 + \exp[(Y_i - Y_j)/k]}$$

where $k = 0.1$. After randomly selects a neighbor j , agent i replaces its strategy S_i by S_j with probability $P(S_i \leftarrow S_j)$. $Y_i = X_i \times A_i$ is established based on

$$X_i = \begin{pmatrix} D_{i1}(1) & \cdots & D_{i,i-1}(1) & D_{i,i+1}(1) & \cdots & D_{iN}(1) \\ D_{i1}(2) & \cdots & D_{i,i-1}(2) & D_{i,i+1}(2) & \cdots & D_{iN}(2) \\ \vdots & \vdots & \vdots & \vdots & \vdots & \vdots \\ D_{i1}(m) & \cdots & D_{i,i-1}(m) & D_{i,i+1}(m) & \cdots & D_{iN}(m) \end{pmatrix},$$

$$Y_i = (Y_i(1), Y_i(2), \dots, Y_i(m))^T,$$

$$A_i = (x_{i1}, \dots, x_{i,i-1}, x_{i,i+1}, \dots, x_{iN})^T,$$

where $D_{ij} = S_j^T(t) P S_j(t)$. Y_i can be obtained directly from payoff data, and A_i can be calculated from strategy recordings. The objective function is

$$\min_{X_i} \left(\frac{1}{2} \|X_i A_i - Y_i\|_2^2 + \lambda_1 \|A_i\|_0 \right),$$

where $\lambda_1 \geq 0$ is a coefficient used to balance the empirical error term and the regularization term. If $\lambda_1 = 0$, the regularization term disappears, the empirical error term dominants and overfitting frequently occurs. As λ_1 increasing, the penalty for model complexity rises. It is an NP hard problem and difficult to solve directly. In the condition of restricted isometric property (RIP), l_0 -norm can be replaced by l_1 -norm:

$$\min_{X_i} \left(\frac{1}{2} \|X_i A_i - Y_i\|_2^2 + \lambda_1 \|A_i\|_1 \right),$$

where $\|A_i\|_1 = \sum_{j=1}^N |a_{ij}|$.

Methods

Solution of Least Squares Method.

$$Y_{node} = f(A_{node} X_{node}) = A_{node} X_{node}$$

$$\min \sum_{i=1}^M v_i \text{loss}_i + g(\mathbf{v}; \lambda) = \sum_{i=1}^M \frac{1}{2} v_i (f(X_i A_i) - Y_i)^2 + g(\mathbf{v}; \lambda) = \sum_{i=1}^M \frac{1}{2} v_i (X_i A_i - Y_i)^2 + g(\mathbf{v}; \lambda)$$

The corresponding close-formed solution is showed as follows:

$$v_i^* = \arg \min_{v_i \in [0,1]} v_i \text{loss}_i + g(v_i; \lambda), i = 1, 2, \dots, M$$

$$A^* = \arg \min_X \frac{1}{2} \sum_{i=1}^M v_i (X_i A_i - Y_i)^2 = \frac{1}{2} \arg \min_X \text{tr} \left\{ [(XA - Y)^T (XA - Y)]_* \begin{bmatrix} v_1 & 0 & 0 \\ 0 & \ddots & 0 \\ 0 & 0 & v_M \end{bmatrix} \right\}$$

$$= [X^T (X_* \mathbf{v})]^{-1} [X^T (Y_* \mathbf{v})]$$

$$\text{If } g(\mathbf{v}; \lambda) = -\lambda \sum_{i=1}^M v_i, \text{ then } v_i^* = \begin{cases} 1, & \text{if } \text{loss}_i < \lambda \\ 0, & \text{otherwise} \end{cases}$$

$$\text{If } g(\mathbf{v}; \lambda) = \frac{1}{2} \lambda \sum_{i=1}^M (v_i^2 - 2v_i), \text{ then } v_i^* = \begin{cases} 1 - \text{loss}_i / \lambda, & \text{if } \text{loss}_i < \lambda \\ 0, & \text{otherwise} \end{cases}$$

LASSO.

$$\min \sum_{i=1}^M v_i \text{loss}_i + \alpha \|X\|_1 + g(\mathbf{v}; \lambda) = \sum_{i=1}^M \frac{1}{2} v_i (f(X_i A_i) - Y_i)^2 + \alpha \|A\|_1 + g(\mathbf{v}; \lambda)$$

$$= \sum_{i=1}^M \frac{1}{2} v_i (X_i A_i - Y_i)^2 + \alpha \|A\|_1 + g(\mathbf{v}; \lambda)$$

The corresponding close-formed solutions are shown as follows:

$$\begin{aligned}
v_i^* &= \arg \min_{v_i \in [0,1]} v_i \text{loss}_i + g(v_i; \lambda), i = 1, 2, \dots, M \\
X^* &= \arg \min_X \frac{1}{2} \sum_{i=1}^M v_i (X_i A_i - Y_i)^2 + \alpha \|X\|_1 \\
&= \arg \min_X \frac{1}{2} \text{tr} \left\{ [(XA - Y)^T (XA - Y)] .* \begin{bmatrix} v_1 & 0 & 0 \\ 0 & \ddots & 0 \\ 0 & 0 & v_M \end{bmatrix} \right\} + \alpha \|A\|_1
\end{aligned}$$

STRidge.

$$\begin{aligned}
\min \sum_{i=1}^M v_i \text{loss}_i + \alpha \|X\|_2^2 + g(\mathbf{v}; \lambda) &= \sum_{i=1}^M \frac{1}{2} v_i (f(X_i A_i) - Y_i)^2 + \alpha \|A\|_2^2 + g(\mathbf{v}; \lambda) \\
&= \sum_{i=1}^M \frac{1}{2} v_i (X_i A_i - Y_i)^2 + \alpha \|A\|_2^2 + g(\mathbf{v}; \lambda)
\end{aligned}$$

The corresponding close-formed solutions are shown as follows:

$$\begin{aligned}
v_i^* &= \arg \min_{v_i \in [0,1]} v_i \text{loss}_i + g(v_i; \lambda), i = 1, 2, \dots, M \\
X^* &= \arg \min_X \frac{1}{M} \sum_{i=1}^M v_i (X_i A_i - Y_i)^2 + \alpha \|X\|_2^2 \\
&= \arg \min_X \frac{1}{M} \text{tr} \left\{ [(XA - Y)^T (XA - Y)] .* \begin{bmatrix} v_1 & 0 & 0 \\ 0 & \ddots & 0 \\ 0 & 0 & v_M \end{bmatrix} \right\} + \alpha \|A\|_2^2 \\
&= [X^T (X .* \mathbf{v}) + M\alpha I]^{-1} [X^T (Y .* \mathbf{v})]
\end{aligned}$$

Primal-dual interior point method. It is not necessarily advantageous to have more training data. The increase of data size may lead to serious accumulation of errors in numerical computation, thus reducing the precision of the algorithm. An appropriately small amount of data can reduce the storage space and computational complexity and improve the accuracy and efficiency. In practical applications, the scale of the dataset should be designed according to the size and complexity of the specific problem. Here, the adjacency matrix of the network is sparse and the performance of the primal-dual interior point method may be improved by properly reducing the amount of training data. We weight all the data by the loss in each iteration, according to which we roughly select some available data and then use the primal-dual interior point method. As the reconstruction results being closer to the ground truth, the loss of clean data is more centralized and compact and then the content of clean data in the selected data is higher, which plays the role of filtering noisy data.

Performance Measurement

We measured AUC score to traditionally quantify the inferences. In particular, the success rates for existent links (SREL) and null connections (SRNC) are separately studied to further characterize the performance of reconstruction. The closer these metrics are to 1, the more perfect inference it is. The reconstructed adjacency matrix is denoted as W^{learn} , and the ground truth adjacency matrix is denoted as W , with the subscript representing the corresponding adjacency vector of node i .

AUC. We use W^{learn} , W , and the toolkit perfcurve function in matlab to calculate the receiver operating characteristic (ROC) curve.

SREL. $(\sum_{i=1}^N \text{sum}(W_i^{\text{learn}} .* W_i) / \text{sum}(W_i)) / N$

SRNC. $(\sum_{i=1}^N \text{sum}((\mathbf{1} - W_i^{\text{learn}}) .* (\mathbf{1} - W_i)) / \text{sum}(\mathbf{1} - W_i)) / N$

Dataset

Model-free network inference from noisy data. In terms of simulated dynamics of gene regulation and kuramoto-like oscillators, we extract time series under minimal sampling condition as $m=5$ time points from $S=50$ different trajectories of network ZK and the directed random network that consists 25 nodes with 4 incoming connections per unit. The DREAM4 in silico network inference challenge provides time courses showing how the gene regulatory network responds to

the appearance and the removal of a perturbation. For networks of size 10, the files contain 5 different time series with 21 time points, while the file number is 10 for networks of size 100. Moreover, Millar 10 is a stochastic simulation (using the Gillespie method) of the Arabidopsis thaliana circadian clock model.

Model-based network inference from noisy data.

Evolutionary Game model

The EG process was repeated 6 times, with 10 rounds played each time. By default, the settings of the simulated time series are as follows:

- 1) noise_free: clean data.
- 2) noise_v1: add random noise by row, the probability is 0.5, the method of calculation in python is $\text{Noise} * \text{random.random}((1, N))$, where the noise intensity Noise is 10.
- 3) noise_v2: Noise = $10 * \text{random}$, the other settings are consistent with noise_v1.
- 4) noise_v3: the global noise added to the overall data, i.e. $\text{Noise} * \text{random.random}((m, N))$, where m is the length of time series. Set Noise as 1, 5, and 10, then average the results.

Epidemic spreading in the human society

To simulate the dynamics, we set the initial partition of infected individuals as 0.5. For clean data, we reserve 50,000 time steps until all nodes are in a susceptible state, while the default time series length is $N * 100$ for noisy data.

CP: For an arbitrary node i , the infection probability λ_i is $(0.7 + 0.2 * \text{rand})$ by default and the probability of recover from infected state is $(0.2 + 0.2 * \text{rand})$, where rand is a random decimal.

SIS: For an arbitrary node i , the infection probability λ_i is $(0.2 + 0.2 * \text{rand})$ by default and the probability of recover from infected state is $(0.4 + 0.2 * \text{rand})$.

- 1) noise_v1: the binary time series of 10% nodes are missing.
- 2) noise_v2: each record is misremembered in terms of the probability 0.1, i.e. 0 and 1 are reversed.

Parameter Settings

ARNI. The optimum selection of basic functions in each case is determined by grid search from A to D as follows:

- A. $h_{ij,p}^i(x_i, x_j) = (x_j - x_i)^p$
- B. $h_{ij,p}^i(x_i, x_j) = \sin(p(x_j - x_i))$ and $h_{ij,p}^i(x_i, x_j) = \cos(p(x_j - x_i))$
- C. $h_{ij,p_1 p_2}^i(x_i, x_j) = x_i^{p_1} x_j^{p_2}$
- D. $h_{ij,p}^i(x_i, x_j) = 1 + \|\mathbb{X}_{ij} - \mathbb{X}_{ij,p}\|^2$, $\mathbb{X}_{ij} = (x_i, x_j)$ and $\mathbb{X}_{ij,p} = (x_{i,p}, x_{j,p})$

Maximum order of the basis expansion is selected from 4 to 10.

Stopping criterium: decrease it to recover longer list of possible links, and the threshold value is set as 0.01.

LASSO. The regularization parameter α has generally been put at 0.01, and the max training epoch is set as 3000.

STRidge. the hyper-parameter α has generally been set as 0.01 or 100.

The hyper-parameter λ in self-paced regularizer is selected from interval [0.0001, 2.5].

Parameter of Networks

dir: directed, undir: undirected.

Name	N	L	dir/undir	Description
ZK	34	78	undir	Social network of a karate club
football	115	613	undir	The network of American football games
dolphin	62	159	undir	Social network of dolphins
jazz	198	2742	undir	Collaboration network of jazz musicians

ER	40	79	undir	Erdős-Rényi random network
BA	40	76	undir	Barabási-Albert scale-free network
WS	40	80	undir	Watts-Strogatz small-world network
NW	40	101	undir	Newman-Watts small-world network
Random	25	100	dir	Random network with fixed number of incoming connections
Millar10	7	15	dir	Arabidopsis thaliana circadian clock
Insilico10	10	—	dir	DREAM4 in silico network
Insilico100	100	—	dir	DREAM4 in silico network

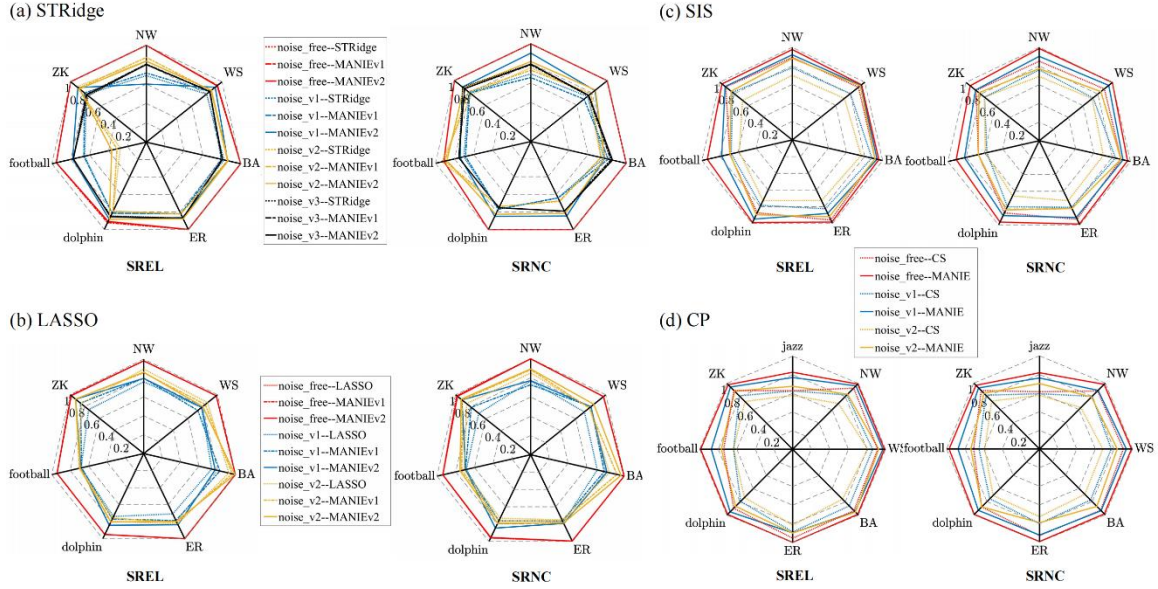


Fig. S1. displays the results for various scenarios: (a) SRELs and SRNCs for model-based inference from EG data using the MANIE framework with embedded STRidge. Here, we employ three real-world networks: ZK, football, and dolphin. Additionally, we utilize four synthetic networks with 40 nodes each: ER, BA, NW, and WS. (b) SRELs and SRNCs for model-based inference from EG data using the MANIE framework with embedded LASSO. (c) SRELs and SRNCs for model-based inference of propagation networks for SIS dynamics using the MANIE framework with embedded primal-dual interior point method. CS represents reconstruction with the primal-dual interior point method. (d) SRELs and SRNCs for model-based inference of propagation networks for CP dynamics using the MANIE framework. The symbolism aligns with scenario (c). These results offer insights into the performance of different methods under diverse conditions.

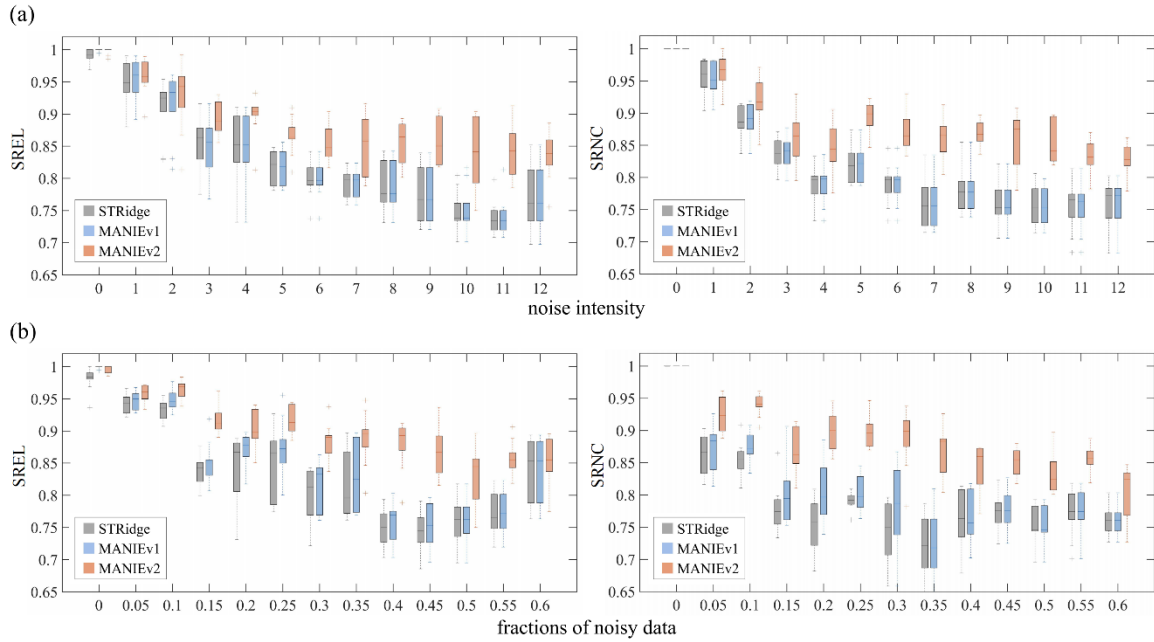


Fig. S2. demonstrates the influence of noise levels on MANIE in the context of ZK network reconstruction. (a) SRELs and SRNCs for model-based inference from EG data using the MANIE framework with embedded STRidge, varying by noise intensity while maintaining a 0.5 fraction of noisy data. (b) SRELs and SRNCs for model-based inference from EG data using the MANIE framework with embedded STRidge, varying by the fraction of noisy data while keeping the noise intensity at 10. The EG process underwent 6 repetitions, each encompassing 10 rounds.

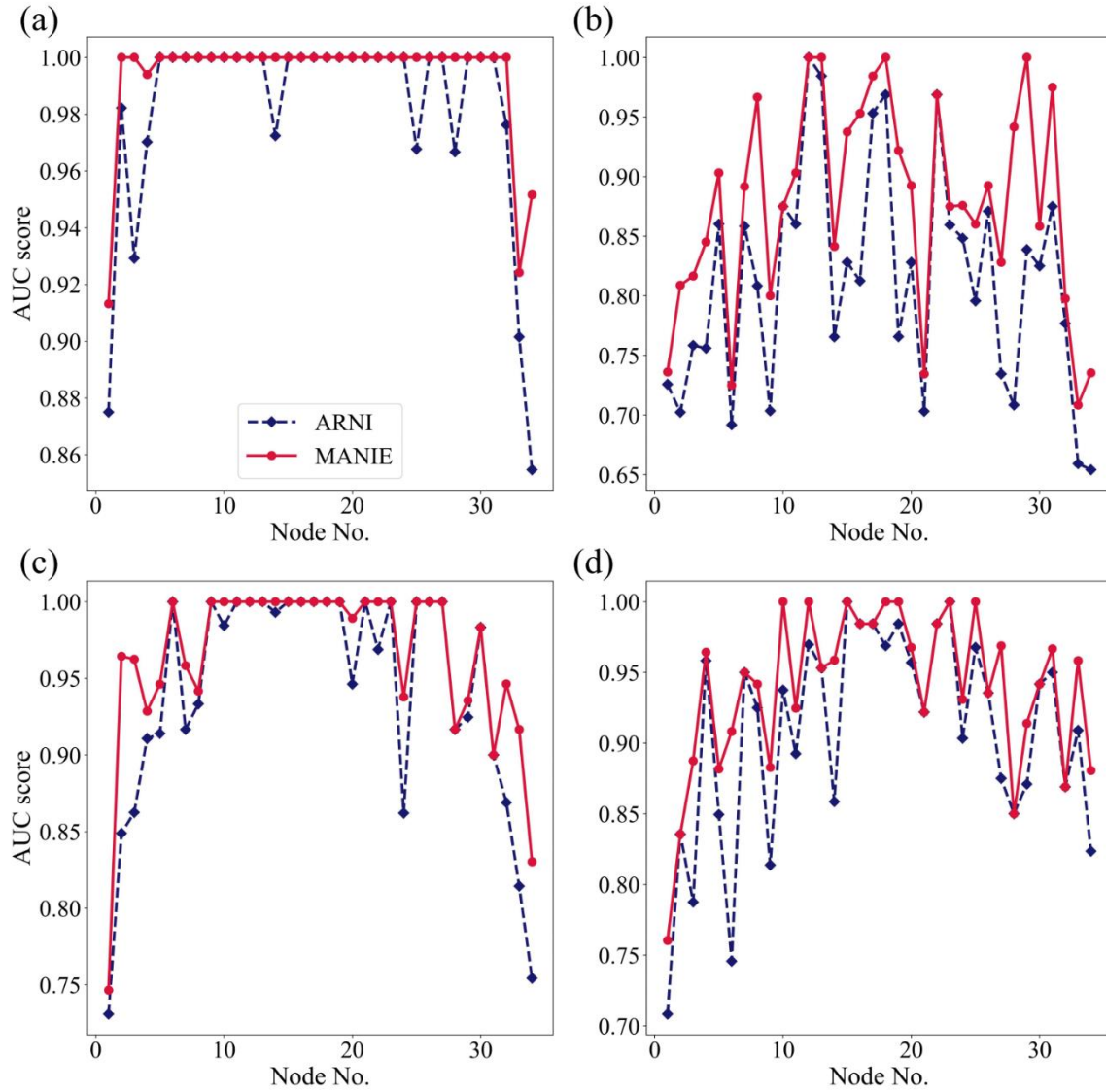


Fig. S3. displays the AUC scores of each node for model-free inference in the context of ZK network from noisy data in various scenarios: (a) Clean data. (b) White Gaussian noise is added to the global time series with a SNR of 10. (c) Each timestep the data is recorded, there is white Gaussian noise in terms of the probability 0.5, and the SNR is 10dB. (d) Each timestep the data is recorded, there is white Gaussian noise in terms of the probability 0.5, and the SNR is 10 dB times a random decimal number from 0 to 1. Each type of data source is simulated under a Kuramoto-1 oscillator.

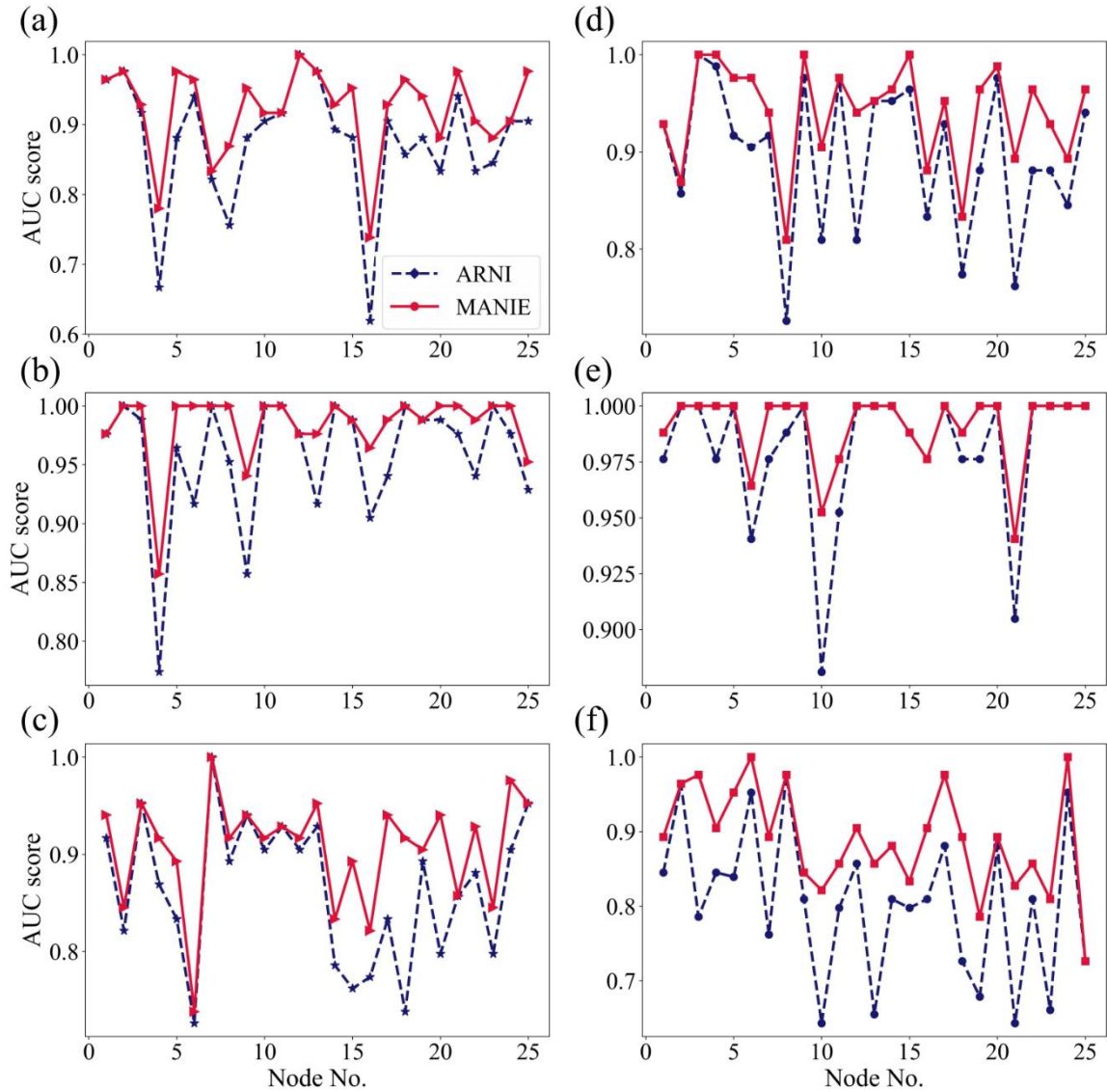


Fig. S4. displays the AUC scores of each node for model-free inference in the context of directed Random network from noisy data in various scenarios: (a, d) White Gaussian noise is added to the global time series with a SNR of 10. (b, e) Each timestep the data is recorded, there is white Gaussian noise in terms of the probability 0.5, and the SNR is 10dB. (c, f) Each timestep the data is recorded, there is white Gaussian noise in terms of the probability 0.5, and the SNR is 10 dB times a random decimal number from 0 to 1. (a-c) Each type of data source is simulated under a Kuramoto-1 oscillator. (d-f) Each type of data source is simulated under a Kuramoto-2 oscillator.

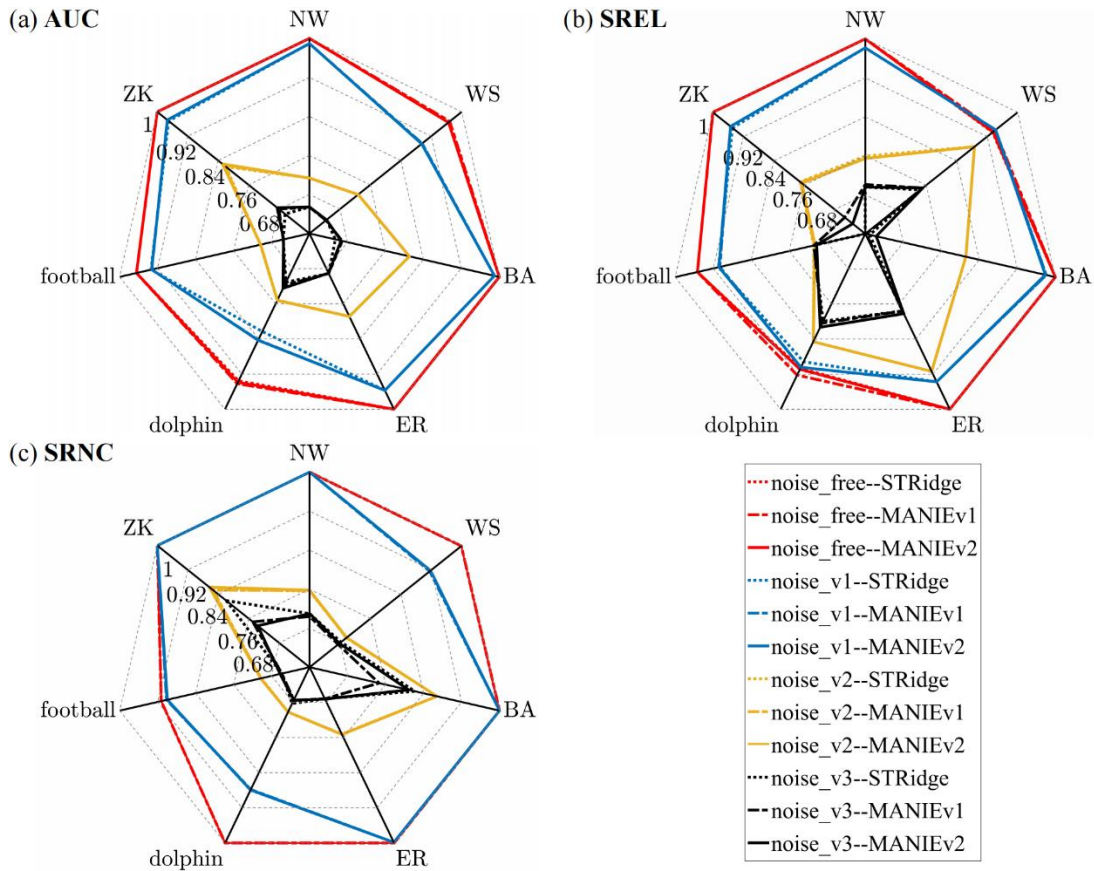


Fig. S5. displays the results for model-based inference from EG data using the MANIE framework with embedded STRidge. We employ three real-world networks: ZK, football, and dolphin. Additionally, we utilize four synthetic networks with 40 nodes each: ER, BA, NW, and WS. Here, noise_free signifies time series without noise, while noise_v1, noise_v2, and noise_v3 represent different levels of noise addition. The suffix of noise_v1 represents that the random noise is added to the global time series with the magnitudes as 1. The suffix of noise_v2 represents that the random noise is added to the global time series with the magnitudes as 5. The suffix of noise_v3 represents that the random noise is added to the global time series with the magnitudes as 10. The EG process underwent 6 repetitions, each encompassing 10 rounds.

SI References

1. Z. Shen, W.-X. Wang, Y. Fan, Z. Di, and Y.-C. Lai, Reconstructing propagation networks with natural diversity and identifying hidden sources, *Nat. Commun.* 5, 4323 (2014).